Thermal degradation of formamidinium based lead halide perovskites into sym-triazine and hydrogen cyanide observed by coupled thermogravimetry-mass spectrometry analysis

Thermal degradation of formamidinium based lead halide perovskites into *sym*-triazine and hydrogen cyanide observed by coupled thermogravimetry - mass spectrometry analysis

Emilio J. Juarez-Perez*, Luis K. Ono, Yabing Qi*

*e-mail: ejjuarezperez@gmail.com; Yabing.Qi@OIST.jp

Energy Materials and Surface Sciences Unit (EMSSU), Okinawa Institute of Science and

Technology Graduate University (OIST), 1919-1 Tancha, Onna-son, Okinawa 904-0495, Japan

ABSTRACT: The thermal stability and decomposition products of formamidinium, a widely used organic cation in perovskite solar cells formulation, were investigated. Thermal degradation experiments of formamidinium-based perovskite and their halide precursors were carried out in helium and vacuum atmosphere at a constant heating rate (20 ºC/min). In addition, pulsed heating steps were employed under illumination/dark conditions to simulate a more realistic working temperature conditions of photovoltaic devices. The identification of decomposition gas products was based on the quadrupole mass spectrometry technique. The released amounts of *sym*-triazine, formamidine, and hydrogen cyanide were observed to highly depend on temperature. For the experimental conditions used in this study, *sym*-triazine was obtained as thermal product of degradation for temperatures above 95ºC. Below this temperature, only formamidine and hydrogen cyanide generation routes were observed. The energy pathways of formamidinium thermal degradation under photovoltaic working temperature conditions were further assessed from density functional theory calculations, and a mechanism for the decomposition was proposed. The results indicated that formamidinium was more resilient to thermal degradation and release of irreversible decomposition products compared to methylammonium. These were attributed due to larger enthalpy and activation energy for decomposition reactions and the absence of irreversible and detrimental thermal degradation reaction pathways exhausting FA organic cation at low temperature.
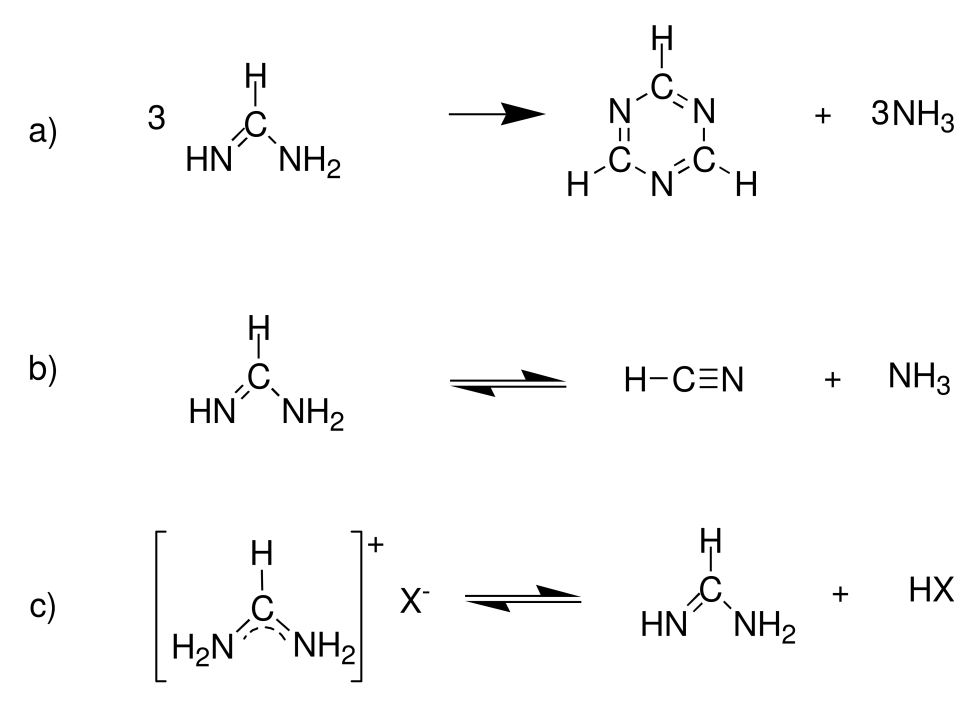
Introduction

A primary concern for perovskite solar cells (PSCs) commercialization is the lack of long-term stability rivaling the well-established silicon based photovoltaic technology.[1-4] Recently, attention to improve the intrinsic stability of this light harvester material has focused on the strategy of employing multi halides and cations mixed compositions instead of pure phase ones. It has been proposed that these halides and cations mixed solid solution phase is stabilized by high configurational/mixing entropy.[5-10] Besides, a trend exists in employing an higher content of formamidinium (FA) cation and minimizing the methylammonium (MA) content in the chemical formulation of hybrid perovskites.[11, 12]

Hybrid perovskites are a special class of semiconductors where the organic cation plays an indirect, but fundamental role in templating the $[PbX_3]^-$ octahedral connectivity. However, the organic cations in these materials could be volatilized at a relatively low thermal stress.[13] Degassing of organic components in hybrid (organic-inorganic) lead halide perovskites at photovoltaic (PV) working temperature conditions is considered one of the most important intrinsic reasons for failure in this emerging PV material.[14] Hybrid perovskite materials must be thermally stable at normalized thermal stress tests that can reach temperatures around 85 ºC. Therefore, encapsulation of these materials is necessary not only to avoid the ingress of third parties agents (oxygen, moisture) that leads to degradation but also to avoid the loss of the organic components by evaporation during the long-term operation of the device. Once the light harvester is encapsulated, it is expected that a small portion of the organic component is released in gas phase during solar cell operation in day time and this gas phase would condensate reversibly within the hermetically sealed cell during the cooler hours at night. In this scenario, crystallization would take place regenerating to perovskite material ready to work the next day.[15, 16] This self-healing mechanism of hybrid perovskites need absence of detrimental irreversible reactions that exhaust the organic components.[13]

In our previous work, we have described the existence of both reversible (CH_3NH_2 + HX) and irreversible (CH_3X + NH_3) photo-, thermal-decomposition reactions in $MAPbI_3$ perovskite material. The release of CH_3X + NH_3 was initially observed during high temperature degradation tests.[17] Recently, it has been found that both degradation routes take place simultaneously near ambient temperature and vacuum conditions.[13] The minority release of CH_3I + NH_3 is understood as a thermodynamically favored path of degradation and the majority CH_3NH_2 + HX release is a kinetically favored route.[18] The latter may not be the ultimate degradation pathway because CH_3NH_2

+ HX is prone to back formation of methylammonium halide (MAX) in closed systems by acid-base neutralization reaction. Meanwhile $CH_3X + NH_3$ does not react back selectively to MAX.[19]

In contrast, the released gas products during thermal degradation of FA are still not well-characterized.[12] The degradation products of FA in hybrid perovskites were first reported early in 2013 by Stoumpos et al.[20] They observed in the course of bulk synthesis in solution of $FAPbI_3$ a large amount of by-product NH_4PbI_3. Later, it was confirmed that the quantity of NH_4PbI_3 generated is severely affected by the cooling rate used during the precipitation stage.[21] Both works inferred indirectly the formation of *sym*-triazine as the decomposition product of FA because such decomposition also releases NH_3 (see Scheme 1.a), which later is protonated giving rise to ammonia cation derivative observed as NH_4PbI_3. Previously, the thermal decomposition of FACl was investigated by Schaefer et al. during the bulk preparative method for the synthesis of *sym*-triazine in high yield.[22] It was established that a certain portion of formamidine molecule follows the "nitrile" route thermal decomposition, which implies HCN (hydrogen cyanide) formation from formamidine, see Scheme 1.b. The interesting point here is that such a route also generates NH_3 as by-product. Therefore, the presence of NH_4PbI_3 contaminant implies formamidinium degradation but does not provide hints about if this degradation was through route a) or b) (or both) in Scheme 1.

Scheme 1. Thermal decomposition reaction of formamidine generating a) *sym*-triazine and b) HCN. c) Reverse of the acid (HX) / base (formamidine) neutralization for the formation of formamidinium halide salt FAX, (X=Br, I).

3

In this work, we investigated by quadrupole mass spectrometry technique the thermal decomposition and evaporation-like gas products released from formamidinium based hybrid perovskites at temperatures relevant for PV devices. Additional high temperature degradation tests facilitated the identification of thermodynamic and kinetic products of decomposition of FA cation. Besides, the activation energy of the first mass loss step (loss of the organic part) was estimated from non-isothermal analysis and compared with MA- and pure inorganic Cs-based perovskites. Density functional theory (DFT) calculations on thermal decomposition routes for FA and MA cations addressed the relative chemical stability of these cations in the corresponding perovskites.

Results and Discussion

Preamble about thermal degradation tests in relation to chemical stability of the material.

All degradation tests carried out in this work (high and low temperature tests) were designed for the purpose of inducing temperature-dependent degradation of the material under inert atmosphere in absence of water, oxygen, and other external stimuli that mimic perovskite material being under real working conditions in solar cells. Thus, the material is not exposed to voltage bias. A chemically-inert sample container with a wide band gap, quartz or alumina, is used to heat and allow simultaneously light-induced degradation studies in perovskite materials. Therefore, all stability trends observed in this work regard to FA based perovskite in relation to its intrinsic chemical stability and without interference with the above third party vectors of degradation. It is assumed that such third party vector of degradation could accelerate the degradation but they cannot improve the intrinsic chemical stability of the material.

Constant rate heating test for high temperature decomposition of FA-based perovskite.

Quadrupole mass spectrometry/Thermal gravimetric and differential thermal analysis (MS/TG-DTA) tandem coupled experiments were conducted for $FAPbI_3$ and $FAPbBr_3$. Non-isothermal constant heating rates of 5, 10, 20 ºC/min were employed in our experiments (see SI file). Unless stated, because the thermodynamic processes were found to be independent of the heating rate, we discuss our results of 20 ºC/min data. Further details of our setup can be found elsewhere.[17] Both hybrid perovskites showed similar two-step mass loss traces indicating the loss of the organic part

formamidinium followed by inorganic halide PbX_2 (X = Br or I) loss above 400 ºC, see top panels in Figure 1 (TG results). Mass spectra of evolved gases during the first mass loss step showed similar pattern of mass to charge ratios independently of the halide composition in perovskite $FAPbI_3$ or $FAPbBr_3$. The main mass-to-charge ratio (m/z) peaks detected were: 81, 54, 44, 27 and 17 m/z ratios amu ascribed to *sym*-triazine molecular peak, HCN(H)CN major fragment of *sym*-triazine, formamidine, HCN, and ammonia molecular peak, respectively (see fragmentation patterns m/z peaks deposited as Figure S8 in SI file). The gas composition considering only molecular peaks for *sym*-triazine, HCN and formamidine was 43±4, 29±4 and 27±2 %, respectively. Irrespective of halide, *sym*-triazine was found to be the majority product released during high temperature degradation tests. A relevant difference between $FAPbI_3$ and $FAPbBr_3$ high temperature thermal decomposition test was the temperature threshold for gas release, 332 ºC in the case of $FAPbI_3$ and 318 ºC in the case of $FAPbBr_3$. Furthermore, we observed the same gas product composition for thermal degradation of FAI (formamidinium iodide) and FAac (formamidinium acetate) applying the above thermal degradation protocol (see Figure S1 and S2 deposited SI file). These experiments confirmed *sym*-triazine to be the major product released at high temperature which could be considered the thermodynamic product for decomposition of the organic part in FA-based perovskite or FAX in the high temperature degradation tests.
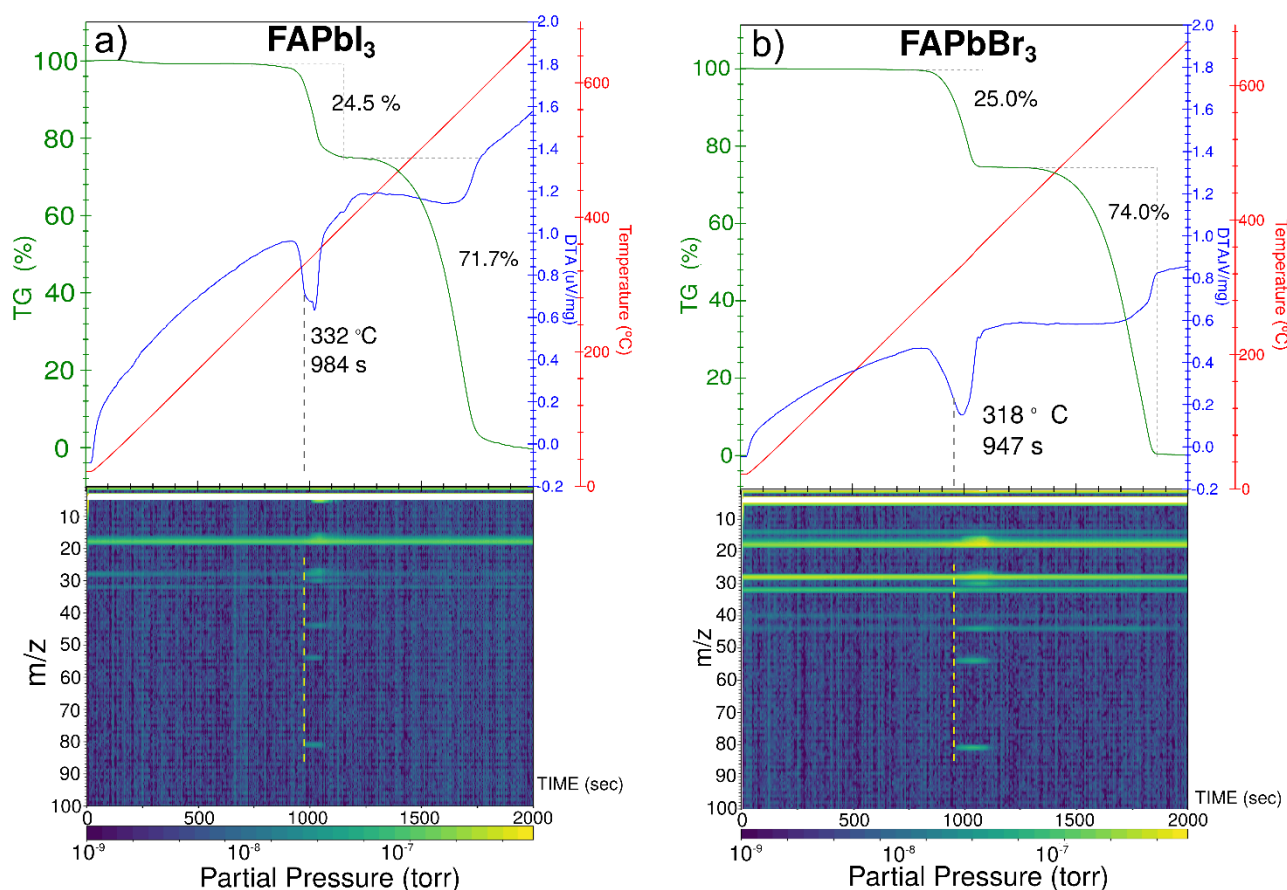
Figure 1. Tandem TG-DTA/MS coupled experiments for a) the FAPbI$_3$ and b) FAPbBr$_3$ hybrid halide perovskites. Top panels show the archetypal two-step type mass loss TG pattern (green line) for hybrid perovskites. Bottom panels show MS traces simultaneously recorded (1-100 amu) during the experiment. Gray dash line indicates the initial temperature (time) of the first detection of released gases during the high-temperature thermal degradation. Full MS spectra (1-200 amu) deposited in SI (Figure S3).

Determination of activation energy for the high temperature thermal decomposition of organic component of FA based perovskites

Thermal analysis was applied in the first mass loss step observed in the thermal gravimetric (TG) traces at three different constant heating rates (5, 10 and 20 °C/min, see Figure S4) for FAPbBr$_3$ and an estimation of the activation energy (E$_a$) and turnover ratio (k) was obtained using a model free approximation. This estimation was further refined using nonlinear regression for direct fit of the nth order Prout-Tompkins auto-catalytic model to the experimental data (see Figure S5 in SI file). Table

1 shows activation energy (E_a) and turnover ratio (k) profiles for the FA based perovskites FAPbBr$_3$ and FAPbI$_3$; FAI precursor and MA-, Cs-based perovskites for comparison purposes.

Table 1. Activation energy (E_a) and turnover ratio (k) for the first mass loss step observed (FA- and MA-based perovskites) during induced thermal degradation.

		E_a (kJ mol^{-1})	log k (s^{-1})
perovskite	FAPbI$_3$	115 ± 3	6.9 ± 0.2
	FAPbBr$_3$	133 ± 1	9.8 ± 0.1
	MAPbI$_3$	93 ± 8	5.6 ± 0.8
	MAPbBr$_3$	98 ± 4	6.1 ± 0.4
	CsPbI$_3^\ddagger$	650 ± 90	33 ± 5
FA precursors‡	FAI	77 ± 1	4.6 ± 0.1
	FABr	52 ± 1	2.0 ± 0.1
	FAac	68 ± 1	5.0 ± 0.1

‡: only single mass loss step observed.

FAPbBr$_3$ has been found to be one of the most stable hybrid lead halide perovskites.[23, 24] According to our thermal analysis, FAPbBr$_3$ had the highest E_a for all hybrid perovskite compositions analyzed, which is followed by FAPbI$_3$. Both FA perovskites had higher E_a than halide equivalent MA counterparts. On the other hand, a pure inorganic (non-hybrid) perovskite as CsPbI$_3$, which only shows a single mass loss step in TG experiment, had the highest E_a compared to organic-inorganic hybrid ones. FA precursors also were studied for comparison purposes showing significantly lower E_a than FA perovskites. Interestingly, the E_a trend observed here for the hybrid perovskites matches well the stability trend obtained for a recent published benchmarking protocol using two figures of merit.[24] Therefore, E_a could also be used as a simplified figure of merit test to assess the chemical (thermal) stability of hybrid perovskites.

Determination of gases evolved from FA-based perovskite during low temperature (< 100 ºC) degradation tests.

The most stable hybrid and FA-based perovskite material – FAPbBr$_3$, as found on the basis of the high temperature stress tests above – was stressed thermally under conditions close to PV working temperatures. Two kinds of heating stimulus were employed consisting of heating pulses in dark or mild illumination pulses to raise temperature and discern between photo- or thermal-assisted releases of gases. The corresponding MS spectra were analyzed tracking the sample temperature recorded under such dark or light conditions, see Figure 2.a.

Under mild light pulses (0.55 Sun), the temperature of the sample reached 60 ºC at maximum peak and the mass spectra showed only mass to charge ratios molecular or fragment peaks related to degasification of FA-based perovskite as formamidine (m/z = 44 amu), HCN (m/z = 27 amu) and NH$_3$ (m/z = 17 amu), see Figure 2.b and Figure S6-7. In contrast, the sample with pulsed heating steps under dark conditions reached temperatures above 75 ºC and four m/z peaks corresponding to the HBr and Br and their isotopes were identified matching the isotopic pattern of ^{79}Br / ^{81}Br ~ 50 / 50% signature for the most abundant isotopes of bromine, see Figure S8d. The release of *sym*-triazine was only observed indirectly with appearance of the fragment m/z = 54 amu (corresponding to the HCN dimer fragment, HCN-(H)CN, Figure S8c) because the *sym*-triazine molecular peak (m/z = 81 amu) overlaps with the HBr / Br isotope peaks. Noticeably, this fragment peak at m/z = 54 amu belonging to *sym*-triazine molecule was only significant during peak temperatures above > 95ºC, Figure 2.c. Therefore, *sym*-triazine can be considered as a high temperature decomposition product of FA not relevant for PV applications and confirmed to be the thermodynamic product of degradation. Instead, formamidine and hydrogen cyanide were observed with formamidine being the majority gas compound observed. The experimental temperature dependent formamidine/HCN ratio is shown in Figure 2.d. There was a noticeably increase of HCN release as temperature raised.

Thus, comparison of degassed products released between both high temperature and PV working temperature tests permitted us 1) to distinguish thermodynamic and kinetic products during thermal degradation of FA and 2) to establish the main reactions releasing the gas components at the working temperature in photovoltaic devices. The foremost relevant fact was a larger release of formamidine + HCN release (74 %) at maximum release of *sym*-triazine compared with the release observed during the high temperature tests (~56 %). It indicated that formamidine formation from formamidinium could be the kinetic product equivalent to methylamine release in methylammonium decomposition. This reaction (Scheme 1.c.) is the reverse of an acid-base neutralization and it is completely reversible

and spontaneous to formamidinium bromide salt back formation. Another main reaction of thermal decomposition observed at PV working temperature would be the release of HCN and ammonia (Scheme 1.b). Fortunately, this reaction is also reversible that leads to back formation of formamidine.[25]
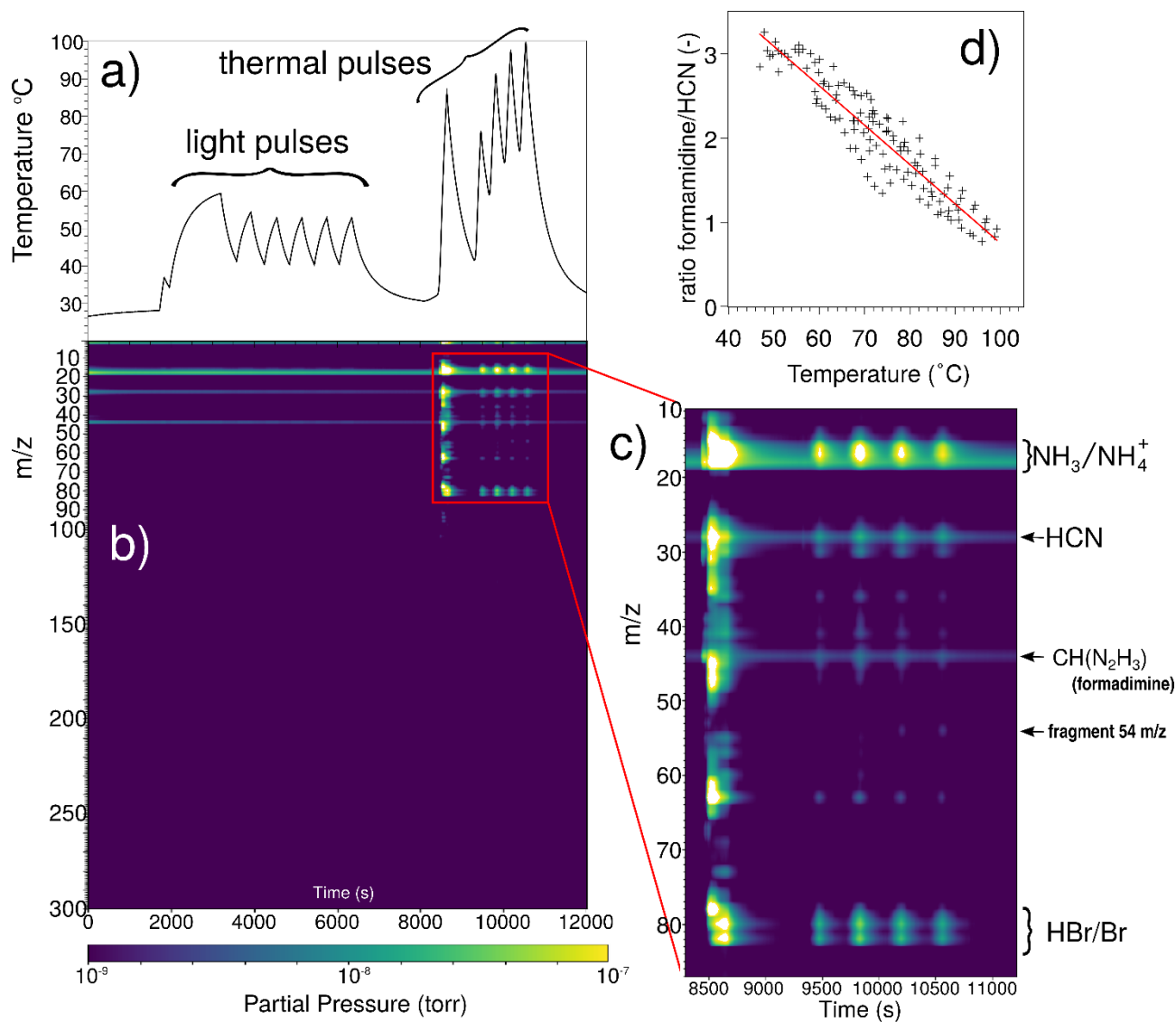

Figure 2. Mass spectrometry profiles of FAPbBr$_3$ decomposition products recorded during illumination and heating-in-the-dark pulsed experiments. a) Sample temperature tracking during light pulses applied using a Xe lamp delivering 55 mW/cm^2 of light power and heating on/off intervals on the sample under dark conditions. b) Time dependent m/z traces registered simultaneously during the thermal degradation under light or dark conditions. c) Inset figure showing the m/z traces during the heating intervals under dark conditions. Species of interest detected in MS are labeled on the right side. d) Experimentally extracted temperature dependent formamidine (m/z = 44 amu) / HCN (m/z =

27 amu) molecular ratio released during controlled degradation of FAPbBr₃. Sensitivity factors for formamidine and HCN are 1.62 and 1.45 considering efficiency of ion transmission expected in the quadrupole mass filter and probability of ionisation proportional to the number of electrons in the sample molecule.

DFT thermochemistry for reactions related to formamidinium thermal decomposition.

Evaluation of reaction thermochemistry involving FA decomposition using DFT was carried out with the ground state of the model compound FAX ionic par (X=Br, I) as the reference. Figure 3 shows the relative enthalpy energy level of the model compound (center) evolving to formamidine and HX where X = Br, I (the reverse of the acid base neutralization; i.e., the left branch in Figure 3; Scheme 1.c); and formation of HCN and NH₄X (right branch in Figure 3; Scheme 1.b and 1.c). For easy comparison, the equivalent reactions for MAX model compound including the methylamine + HX release (left side) and irreversible reaction generating CH₃X + NH₃ (right side) were added in Figure 3.
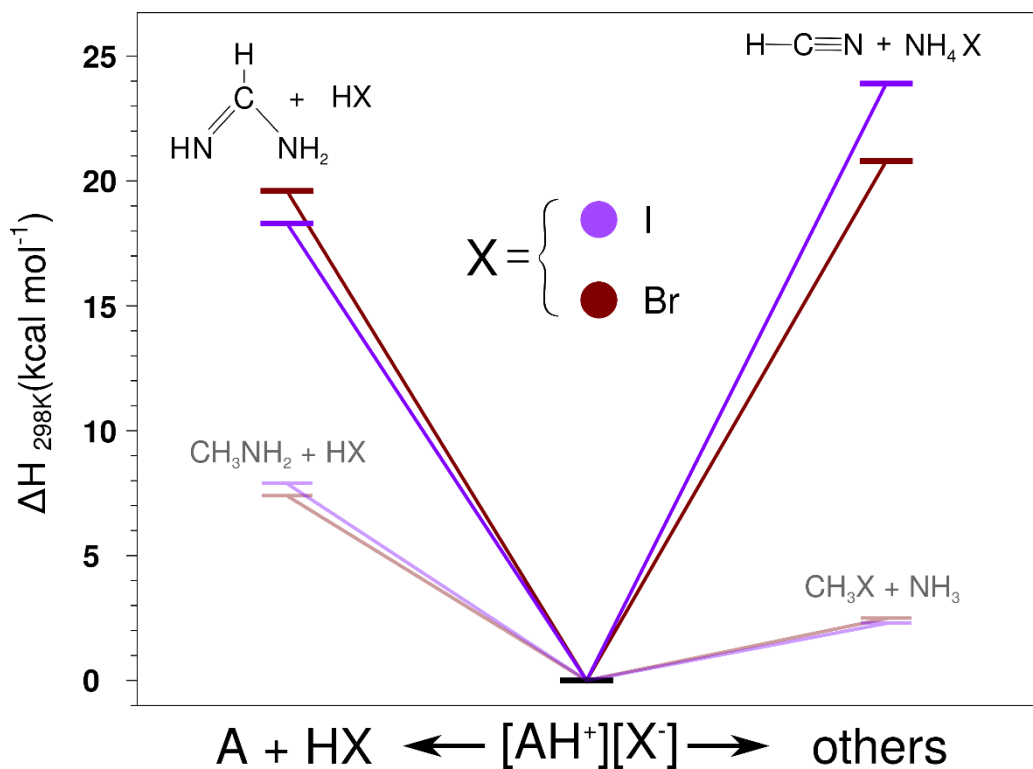
Figure 3. Enthalpy energy level with reference to interacting reactant system $[AH^+][X^-]$ (A = methylamine, formamidine), (X=Br, I) at 25 ºC.

DFT calculations showed that both FA-based reverse acid-base reaction and reversible thermal degradation to HCN + NH_4X had larger reaction enthalpy differences compared to the equivalent degradation/decomposition reactions in the MA cation based systems. This theoretical results evidenced larger robustness for thermal decomposition of FA cation compared to MA cation agreeing the experimental trend observed for activation energy of the first mass loss step for FA and MA based perovskites (see Table 1) and the robustness of FA as organic cation in hybrid perovskites. However, selective contacts and metal electrode in PV devices must be chosen as chemically inert as possible toward volatile released products which can provoke undesired side-reactions.[26] A comparison of the gases released in MA and FA case reveals that the biggest difference is that the former releases a methylating agent (CH_3X). The remaining gaseous components released remain identical (HX and NH_3) except for a stronger base such as formamidine compared to methylamine. Therefore, there is evidence that the rule of chemically inert selective contact[13] in the case of the FA based perovskite will also have to be fulfilled. Finally, hybrid perovskite based photovoltaic field is moving toward more mixed systems which have been shown to improve stability than pure phase ones. It is expected a significant interaction between the different organics released in mixed compositions and it deserves further research on regards of the long term stability of the composite light harvesting material.

Conclusions

The ideal halide perovskite composition, in terms of chemical stability, would be a perovskite that has no organic component at all. However, organic cations offer environmental and economic advantages of easy fabrication and low-cost compared to extraction and purification of inorganic alternative cations such as Cs. Specially, the use of organic FA cation, is convenient due to its larger chemical (thermal) stability and resistance to evaporation compared to the MA cation as demonstrated in this work.

The improved stability of FA compared to MA has been observed from the larger activation energy estimation for the first mass loss step during thermal stress and confirmed by DFT calculations

because of a larger enthalpy exchange necessary to proceed with thermal decomposition reactions. The irreversible degradation product from the thermal degradation of FA is *sym*-triazine but it is only probed by mass spectrometry technique above 95 °C. This temperature is well above the usually considered working temperature range in PV applications. Also, FA cation develops the benign reversible acid-base decomposition (formamidine + HX) similar to the release route for the MA cation (methylamine + HX). Noteworthy, the parallel route for the FA decomposition reaction releasing HCN + NH$_3$ is reversible and it can reversibly back react to form formamidine molecule (formamidinium cation) in strong contrast with the equivalent release of CH$_3$X + NH$_3$, which is not selectively reversible to the back formation of methylammonium. FA meets the requirement of absence of reactions exhausting the cation irreversibly in the range of temperature for PV applications for a satisfactory encapsulation and long-term operation of hybrid perovskite light harvester material.

Experimental Section

Sample preparation

Lead (II) iodide (PbI2, 99.9%) was purchased from Tokyo Chemical Industry Co., Ltd, lead (II) bromide (PbBr2, 99.999%) was purchased from Sigma-Aldrich, formamidinium iodide (FAI) and formamidinium bromide (FABr) reagent grade were purchased from Dyesol Limited and formamidinium acetate (FAac) from Wako Pure Chemical Industries. All chemicals were used as received without any further purification. Hybrid perovskites in powdered polycrystalline form were prepared using ~1 M solutions of stoichiometric precursor quantities to synthesize FAPbI$_3$ and FAPbBr$_3$ using 1 mL of DMF/DMSO (1:1) (Wako Pure Chemical Industries) solvent. The solution is poured on a 10 cm in diameter mortar kept at 100 °C inside fume hood and slowly spread on the mortar surface helped by the pestle. Solvents are evaporated in 1-2 minutes leaving the solid crystalline material on the mortar surface. These hybrid perovskites formulations in powdered polycrystalline material phase were obtained mimicking the procedure to deposit perovskite thin films on substrates.

Experimental setup no. 1. High temperature degradation test using TG-DTA/MS Tandem equipment.

Safety: There is a significant hazard by release of HCN (hydrogen cyanide) during the thermal heating tests. All FA-based materials used during the tests are kept to a minimum quantity and all vacuum pump exhausts are connected to the general exhaust system of the lab.

Simultaneous thermal gravimetric (TG) and differential thermal analysis (DTA) (TG-DTA2000SE, Netzsch) data were recorded in the temperature range from 25 to 700 °C, at heating rates from 5 to 20 °C/min for polycrystalline samples of FAPbI3, FAPbBr3, FAI, FABr and FAac in alumina crucibles and using He as carrier gas (100 mL/min). A portion of the released gases from the TG-DTA apparatus were fed directly into a residual gas analyzer (Hiden Analytical) through a heated Quartz Inert Capillary (QIC) (HPR-20/QIC) and passed through a quadrupole mass filter for mass analysis scanning sequentially from m/z = 1 to 100. The ion flux is measured using a Faraday cup detector. Identical experimental setup was used in reference no. 2.

Experimental setup no. 2. Pulsed low temperature/light irradiation experiments.

Safety: There is a significant hazard by release of HCN (hydrogen cyanide) during the thermal heating tests. All FA-based materials used during the tests are kept to a minimum quantity and all vacuum pump exhausts are connected to the general exhaust system of the lab.

A sample of $FAPbBr_3$ (~150 mg) is placed in a quartz crucible inside a stainless steel vacuum chamber. Once a high vacuum level is reached ($<10^{-6}$ Torr), the pressure gauge and MS spectrometer are switched on. The temperature of the sample under dark conditions and high vacuum conditions was observed to be slightly high (30-35 °C) due to unavoidable heating of the electron ionizer. Simulated sun-light pulses are obtained using a 150 W short-arc Xe lamp from the solar simulator (PEC-L01, Peccell Technologies Inc.). Light pulses in the solar simulator were computer controlled and chopped remotely by a homemade program and actuator. Illumination power delivered by the solar simulator was calibrated using a calibrated silicon photodiode accounting quartz window and distance between light source and sample holder. Mass spectrometer traces were recorded using a quadrupole mass spectrometer (1-300 amu) equipped with an electron multiplier detector (RGA300, SRS Stanford Research Systems).

DFT

DFT ground-state geometry optimizations were carried out using perturbatively corrected double hybrid functional with the Gershom Martin's "thermochemistry" reparametrization B2T-PLYP[27] as implemented in the ORCA 3.0.3 package.[28] Ground-state calculations use minimally augmented diffuse and 0th order regular approximation (ZORA) recontracted scalar relativistic polarized triple zeta basis set (ma-ZORA-def2-TZVP) for all atoms.[29-31]. Frequency calculations were carried out at the same level of theory determining the nature of the stationary points for reactants and product characterized with zero imaginary frequency.

Supporting Information

Tandem TG-DTA/MS coupled experiments for FAI and FAac. Full 1-300 amu m/z MS traces recorded for $FAPbI_3$ and $FAPbBr_3$. Tandem TG-DTA/MS coupled experiments for $FAPbBr_3$ recorded to 5, 10 and 20 ºC/min heating rate. Fittings of TG curves during the first mass loss step. Raw m/z ratio traces (non-calibrated) recorded for NH_3 (17 amu), NH_4^+ (18 amu), HCN (27 amu), N_2^+ (28 amu), formamidine HCN_2H_3 (44 amu) and *sym*-triazine (54 amu) fragment. Blank MS experiment of the empty 6-ways cross chamber recorded during illumination and heating-in-the-dark

pulsed experiments. Fragmentation patterns m/z peaks for ammonia, hydrogen cyanide, *sym*-triazine and hydrogen bromide.

REFERENCES

1. M. A. Green, Y. Hishikawa, E. D. Dunlop, D. H. Levi, J. Hohl-Ebinger and A. W. Ho-Baillie, *Prog. Photovolt. Res. Appl.*, 2019, **27**, 3-12.
2. Y. Yang and J. You, *Nature*, 2017, **544**, 155-156.
3. L. K. Ono, Y. B. Qi and S. F. Liu, *Joule*, 2018, **2**, 10-1016.
4. R. Wang, M. Mujahid, Y. Duan, Z.-K. Wang, J. Xue and Y. Yang, *Adv. Funct. Mater.*, 2019, 1808843.
5. C. Yi, J. Luo, S. Meloni, A. Boziki, N. Ashari-Astani, C. Gratzel, S. M. Zakeeruddin, U. Rothlisberger and M. Gratzel, *Energy Environ. Sci.*, 2016, **9**, 656-662.
6. K. T. Butler, K. Svane, G. Kieslich, A. K. Cheetham and A. Walsh, *Phys. Rev. B*, 2016, **94**, 180103.
7. T. Chen, B. J. Foley, C. Park, C. M. Brown, L. W. Harriger, J. Lee, J. Ruff, M. Yoon, J. J. Choi and S.-H. Lee, *Sci. Adv.*, 2016, **2**, 1601650.
8. N. J. Jeon, J. H. Noh, W. S. Yang, Y. C. Kim, S. Ryu, J. Seo and S. I. Seok, *Nature*, 2015, **517**, 476-480.
9. T. Jesper Jacobsson, J.-P. Correa-Baena, M. Pazoki, M. Saliba, K. Schenk, M. Grätzel and A. Hagfeldt, *Energy Environ. Sci.*, 2016, **9**, 1706-1724.
10. J. Jeon, T. Eom, E. Lee, S. Kim, K.-H. Hong and H. Kim, *J. Phys. Chem. C*, 2017, **121**, 9508-9515.
11. L. K. Ono, E. J. Juarez-Perez and Y. B. Qi, *ACS Appl. Mater. Interfaces*, 2017, 10-1021.
12. S.-H. Turren-Cruz, A. Hagfeldt and M. Saliba, *Science*, 2018, **362**, 449-453.
13. E. J. Juarez-Perez, L. K. Ono, M. Maeda, Y. Jiang, Z. Hawash and Y. B. Qi, *J. Mater. Chem. A*, 2018, **6**, 9604-9612.
14. J. A. McLeod and L. Liu, *J. Phys. Chem. Lett.*, 2018, **9**, 2411-2417.
15. P. Holzhey, P. Yadav, S.-H. Turren-Cruz, M. Grätzel, A. Hagfeldt and M. Saliba, *Mater. Today*, 2018, 10.1016/j.mattod.2018.1010.1017.

16. K. Domanski, B. Roose, T. Matsui, M. Saliba, S.-H. Turren-Cruz, J.-P. Correa-Baena, C. R. Carmona, G. Richardson, J. M. Foster, F. De Angelis, J. M. Ball, A. Petrozza, N. Mine, M. K. Nazeeruddin, W. Tress, M. Grätzel, U. Steiner, A. Hagfeldt and A. Abate, *Energy Environ. Sci.*, 2017, **10**, 604-613.

17. E. J. Juarez-Perez, Z. Hawash, S. R. Raga, L. K. Ono and Y. B. Qi, *Energy Environ. Sci.*, 2016, **9**, 3406-3410.

18. A. Ciccioli and A. Latini, *J. Phys. Chem. Lett.*, 2018, **9**, 3756-3765.

19. E. J. Juarez-Perez, L. K. Ono, I. Uriarte, E. J. Cocinero and Y. B. Qi, *ACS Appl. Mater. Interfaces*, 2019, 10.1021/acsami.1029b02374.

20. C. C. Stoumpos, C. D. Malliakas and M. G. Kanatzidis, *Inorg. Chem.*, 2013, **52**, 9019-9038.

21. W. T. M. Van Gompel, R. Herckens, G. Reekmans, B. Ruttens, J. D'Haen, P. Adriaensens, L. Lutsen and D. Vanderzande, *J. Phys. Chem. C*, 2018, **122**, 4117-4124.

22. F. C. Schaefer, I. Hechenbleikner, G. A. Peters and V. P. Wystrach, *J. Am. Chem. Soc.*, 1959, **81**, 1466-1470.

23. N. Arora, M. I. Dar, M. Abdi-Jalebi, F. Giordano, N. Pellet, G. Jacopin, R. H. Friend, S. M. Zakeeruddin and M. Grätzel, *Nano Lett.*, 2016, **16**, 7155-7162.

24. A. García-Fernández, E. J. Juarez-Perez, S. Castro-García, M. Sánchez-Andújar, L. K. Ono, Y. Jiang and Y. B. Qi, *Small-Methods*, 2018, 1800242.

25. J. Oro, *Nature*, 1961, **191**, 1193.

26. M. B. Islam, M. Yanagida, Y. Shirai, Y. Nabetani and K. Miyano, *Sol. Energy Mater. Sol. Cells*, 2019, **195**, 323-329.

27. T. Schwabe and S. Grimme, *Phys. Chem. Chem. Phys.*, 2007, **9**, 3397‐3406.

28. F. Neese, *Wiley Interdiscip. Rev.: Comput. Mol. Sci.*, 2012, **2**, 73-78.

29. J. Zheng, X. Xu and D. G. Truhlar, *Theor. Chem. Acc.*, 2011, **128**, 295-305.

30. D. A. Pantazis, X.-Y. Chen, C. R. Landis and F. Neese, *J. Chem. Theory Comput.*, 2008, **4**, 908-919.

31. F. Weigend and R. Ahlrichs, *Phys. Chem. Chem. Phys.*, 2005, **7**, 3297-3305.

Graphical Abstract